INVESTIGATION OF TURBULENCE CHARACTERISTICS AND ITS INFLUENTIAL PARAMETRIC OPTIMIZATION OF A DOUBLE-SIDED LID-DRIVEN CAVITY USING TAGUCHI AND ANOVA METHODS

Gnanasekaran MANOGARAN[1], Satheesh ANBALAGAN*

[1,*]Department of Thermal and Energy Engineering, School of Mechanical Engineering,

Vellore Institute of Technology, Vellore, Tamilnadu, India-6323014.

*Corresponding author;E-mail: satheesh.a@vit.ac.in

Abstract

This paper investigates turbulence characteristics and the parameters controlling the turbulent incompressible flow of a double-sided lid-driven cavity. The effects of varying Reynolds numbers ($1\times10^4 \leq Re \leq 2\times10^5$), speed ratios ($0.05 \leq S \leq 1.0$), and aspect ratios ($0.5 \leq K \leq 2.0$) on the turbulent quantities, such as kinetic energy (k), dissipation (ε), turbulent viscosity (ν_t) are analyzed. The k-ε turbulence model equations are solved using the FVM-based SIMPLE algorithm. Taguchi's approach uses an L_{16} orthogonal array to determine the optimal cavity parameters. The significance of the considered factors is estimated using the analysis of variance (ANOVA) method. The present study reveals that the turbulent quantities are significantly reduced by increasing the aspect ratio, speed ratio, and Reynolds number. Taguchi analysis suggests that the optimal fluid flow rate is attained by combining $S = 0.05$, $K = 0.5$, and $Re = 2\times10^5$. The ANOVA analysis shows the significant percentage contribution for parameters S and Re, which are approximately 62.29% and 30.21%, respectively. From the regression equation, $\nu_{t,avg}$ has a positive relationship with both K and Re but a negative relationship with S.

Keywords*:* *Lid-driven cavity; Speed ratio; Aspect ratio; Turbulent Viscosity; Taguchi method; ANOVA.*

1. Introduction

The lid-driven cavity is one of the most prominent problems in determining the flow stability of cellular structures. Double-sided cavities have been studied extensively for their applications in various industrial and technological requirements. This investigation includes solar thermal systems, heat exchangers, room ventilation, building cooling and heating, electronic device cooling, thermal energy storage, geothermal systems, fuel cells, chaotic advection mixing, coating systems, and drying methods [1, 2]. Hammami et al. [3] suggested numerous lid-driven flow cavity applications, including electronic card cooling, food processing, multi-screen nuclear reactor structures, and crystal production. In their research, Shankar et al. [4]investigated lid-driven cavities featuring simple geometric shapes. They observed fluid flow circulating due to the movement of one or more of the walls enclosing the cavity. Both Ghia et al. [5] and Erturk et al.[6] have been widely recognized for

their work on laminar flow with Reynolds numbers of 1×10^4 and 2×10^4 in a square cavity. The study was expanded by Kuhlmann et al. [7] from a single-sided to a double-sided lid-driven cavity. More specifically, they used numerical and experimental methods to investigate two and three-dimensional flows in cavities whose walls move in opposite directions. The results reveal that cavity aspect ratio and sidewall velocities significantly affect vortex formation. Satheesh et al. [8, 9, 10, 11] investigated the double diffusive mixed convection with various possibilities of cavity combinations for laminar flow problems. Their study reveals that an increase in magnetic effect retards the fluid flow. The following section of this article focuses on some of the significant numerical studies of double-sided lid-driven cavities. In a study on a two-sided cavity, Gaskell et al. [12] analyzed stokes flow for a range of speed ratios (-1.0 to 1.0) and aspect ratios (0.5 to 2.0). Wahba et al. [13] numerically investigated double and four-sided cavities in a 2D incompressible flow, and for Re = 10, the flow field generated a symmetric diagonal in both types of driven cavities. Chen et al. [14] used a double-sided cavity with movable walls to investigate the bifurcation for Reynolds numbers (1 to 1200) and aspect ratios (1.0 to 2.5). In a double-sided cavity, Hammami et al. [15] studied the bifurcation phenomena with the combined effect of speed ratio (0.25 to 0.82) and aspect ratio (0.25 to 1.0) in a double-sided cavity, Mendu et al. [16] examined the effects of the Reynolds number, speed ratio, and power-law index on a non-Newtonian fluid in a cavity and found that the drag coefficient rises with the power-law index. At the same time, the generation of secondary vortices is diminished. The following articles address the importance of turbulent flow. Samantaray et al.[17] studied the turbulent flow at high Reynolds numbers inside a cavity with a wide range of aspect ratios between its width and depth. When the spanwise aspect ratio decreases, mean turbulent quantities also decrease due to the higher viscous drag experienced at the end walls. Patel et al. [18] explored incompressible turbulent flow with anti-parallel horizontal walls for Re = 12000. Time series and power spectra were provided for variables like turbulent kinetic energy and production in the region with the most turbulence generation region. A variety of numerical approaches, including the RANS (Reynolds-Averaged Navier-Stokes) model, LES (Large Eddy Simulation) model, and DNS (Direct-Numerical Simulation) model, have been used to analyze turbulent flow behavior to solve various types of problems with different flow configurations. Additionally, many studies have been published using advanced simulation methods to examine turbulent flows in double-sided cavities. The most precise method for simulating turbulent flow uses DNS to resolve the Navier-Stokes equations and obtain a three-dimensional resolution of all turbulence scales. However, DNS is expensive even for low Reynolds number flows over simple geometries. LES can only resolve large eddies in turbulent flow, and while it is less expensive than DNS, most applications still require excessive processing effort and resources. An alternative method for simulating turbulent flow is the RANS model, which can model all length scales of turbulence. In the last few decades, RANS has been used as the basis for the modern CFD method for modeling turbulent flow because it is easier to use and requires less expensive computer equipment [19, 20]. There are only a few numerical studies on turbulent flow at Re greater than 1×10^4 have been published [21, 22, 23]. Therefore, the authors of this work examine the flow behavior for Reynolds numbers between 1×10^4 and 2×10^5. A limited research paper on the parametric optimization involved in turbulent flow is presented. The following article discusses optimization studies in lid-driven flow problems.

Recently, the authors Moolya and Satheesh [24] conducted an optimization study on double-diffusive mixed convection flow using Taguchi analysis and presented the optimal and significant

parameters. Using the Taguchi method, Alinejad and Esfahani [25] optimized the turbulent mixed convection in an enclosure. Taguchi's L_{16} orthogonal array was used to organize the simulations. Finally, it is observed that the Taguchi approach optimized the heat transfer rate accurately. Sobhani and Ajam [26] reported a study on natural convection and Taguchi optimization using an L_{27} orthogonal array. The study found that optimal conditions were achieved. Shirvan et al. [27] investigated the optimization of mixed convection using the Taguchi method. The optimal outlet port position was found to be at 0.9H for a Richardson number of 0.01. Furthermore, a study was carried out to optimize the mixed magnetohydrodynamic convection. The study also considers different positions of the inlet and outlet ports [28]. Alinejad and Fallah [29] used the Taguchi method L_{25} array to optimize the maximum heat transfer in an enclosure. A signal-to-noise ratio analysis was conducted to determine the process parameter effects and optimal factor settings.

According to the above literature, speed ratio [12, 15, 16] is one of the influential parameters even at laminar flow problems. Hence, the present study considers the speed ratio for investigating the turbulent flow in the square-enclosed cavity. According to the authors, no studies have been done on optimizing the controlling parameters in turbulent fluid flow behavior with speed ratio. Optimizing the parameters with the selected range of values offers a significant benefit, dramatically reducing the required number of simulations and the related computational cost. Therefore, in the present numerical investigation, an optimization study is conducted to achieve the maximum fluid flow in the enclosed cavity using Taguchi and ANOVA statistical methods. These two statistical methods examine the optimal combination of the chosen parameters and their levels. It attains a correlation based on the impact of Reynolds number, speed ratio, and aspect ratio on fluid flow characteristics in a cavity.

2. Physical model

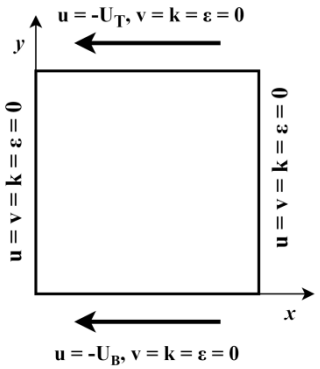

Fig. 1: Mathematical model of the problem

The mathematical model and its boundary conditions used for the present numerical analysis are shown in Fig.1.The domain is filled with incompressible and Newtonian fluid. All of the physical properties related to fluid are taken to be constant. The vertical walls are maintained stationary. The bottom and top walls move at different velocity combinations in the -x direction. The top velocity is $U_{T,}$ and the bottom velocity is U_B. The ratio of these two velocities is called the Speed ratio ($S = U_B / U_T$). Its range is fixed from 0.05 to 1.0. The Reynolds Number (Re) varies from 1×10^4 to 2×10^5, and the aspect ratio (K) varies from 0.5 to 2.0. Due to this range of Reynolds number, the flow inside the cavity is turbulent. The Reynolds decomposition technique uses the RANS and k-ε turbulent

governing equations to resolve the above problem. Boussinessq developed an approximation for the turbulence stresses to mean flow [30], and the following Reynolds stresses $(-\overline{u_i' u_j'})$ are obtained.

$$-\overline{u_i' u_j'} = \vartheta_t \left[\frac{\partial \overline{u_i}}{\partial x_j} + \frac{\partial \overline{u_j}}{\partial x_i}\right] - \frac{2}{3} k \delta_{ij}. \quad (1)$$

Where $\delta_{ij,}$ ν_t ,k are denoted by Kronecker delta, turbulent kinematic viscosity, and turbulent kinetic energy, respectively. After incorporating the boussinessq approximation, the following non-dimensional RANS equations will be obtained as follows:

$$\frac{\partial \bar{U}}{\partial X} + \frac{\partial \bar{V}}{\partial Y} = 0 \quad (2)$$

$$\frac{\partial(\bar{U}\bar{U})}{\partial X} + \frac{\partial(\bar{U}\bar{V})}{\partial Y} = -\frac{\partial}{\partial X}\left[\bar{P} + \frac{2}{3}k\right] + \frac{1}{Re}\frac{\partial}{\partial X}\left[\left(1 + \vartheta_{t,n}\right)\frac{\partial \bar{U}}{\partial X}\right] + \frac{1}{Re}\frac{\partial}{\partial Y}\left[\left(1 + \vartheta_{t,n}\right)\frac{\partial \bar{U}}{\partial Y}\right] \quad (3)$$

$$\frac{\partial(\bar{U}\bar{V})}{\partial X} + \frac{\partial(\bar{V}\bar{V})}{\partial Y} = -\frac{\partial}{\partial Y}\left[\bar{P} + \frac{2}{3}k\right] + \frac{1}{Re}\frac{\partial}{\partial X}\left[\left(1 + \vartheta_{t,n}\right)\frac{\partial \bar{V}}{\partial X}\right] + \frac{1}{Re}\frac{\partial}{\partial Y}\left[\left(1 + \vartheta_{t,n}\right)\frac{\partial \bar{V}}{\partial Y}\right] \quad (4)$$

Where $\bar{U}, \bar{V}, \bar{P}$ and $\vartheta_{t,n}$ are denoted as average velocities in the respective directions, average pressure, and kinematic viscosity, respectively. The following k-ε turbulence model equations are required to calculate the mean flow properties and turbulent quantities proposed by Launder et al. [31]. The turbulent kinetic energy (k) equation can be expressed as;

$$\frac{\partial(\bar{U}k_n)}{\partial X} + \frac{\partial(\bar{V}k_n)}{\partial Y} = \frac{1}{Re}\frac{\partial}{\partial X}\left[\left(1 + \frac{\vartheta_{t,n}}{\sigma_k}\right)\frac{\partial k_n}{\partial X}\right] + \frac{1}{Re}\frac{\partial}{\partial Y}\left[\left(1 + \frac{\vartheta_{t,n}}{\sigma_k}\right)\frac{\partial k_n}{\partial Y}\right] + G_n - \varepsilon_n \quad (5)$$

The terms diffusion, production, and dissipation in Eq. (5) are on the right side of the above equation, respectively, with the advection term on the left side. The dissipation rate (ε) can be expressed as;

$$\frac{\partial(\bar{U}\varepsilon_n)}{\partial X} + \frac{\partial(\bar{V}\varepsilon_n)}{\partial Y} = \frac{1}{Re}\frac{\partial}{\partial X}\left[\left(1 + \frac{\vartheta_{t,n}}{\sigma_\varepsilon}\right)\frac{\partial \varepsilon_n}{\partial X}\right] + \frac{1}{Re}\frac{\partial}{\partial Y}\left[\left(1 + \frac{\vartheta_{t,n}}{\sigma_\varepsilon}\right)\frac{\partial \varepsilon_n}{\partial Y}\right] + C_{1\varepsilon}\frac{\varepsilon_n}{k_n}G_n - C_{2\varepsilon}\frac{{\varepsilon_n}^2}{k_n} \quad (6)$$

$$G = \frac{\vartheta_{t,n}}{Re}\left[2\left[\left(\frac{\partial \bar{U}}{\partial X}\right)^2 + \left(\frac{\partial \bar{V}}{\partial Y}\right)^2\right] + \left(\frac{\partial \bar{U}}{\partial Y} + \frac{\partial \bar{V}}{\partial X}\right)^2\right] \quad (7)$$

According to Launder et al.[31] k- ε model, the turbulent eddy viscosity ($\nu_{t,n}$) is determined by;

$$\vartheta_{t,n} = C_\mu Re \frac{{k_n}^2}{\varepsilon_n} \quad (8)$$

The k-ε model constants used in the above equations are given below (Biswas et al. [30]);

$$\sigma_k = 1.0, \sigma_\varepsilon = 1.30, C_\mu = 0.09, C_{1\varepsilon} = 1.44, C_{2\varepsilon} = 1.92.$$

The viscous sublayer of a boundary layer is thin at high Reynolds numbers, making it difficult to resolve with sufficient grid points. Wall functions depend on the universal law of the wall, which asserts uniform velocity distribution close to a wall. Wall functions (y+) are empirically determined equations used to satisfy physics in the region close to the wall. A fine grid size near the wall is essential for solving the wall layer effectively using a numerical solution technique. The starting computational point p is in the fully turbulent log-law zone near the wall. The following relationships are used to determine the friction velocity (u_τ) proposed by Nallasamy et al.[32].

$$y_p^+ = \frac{y_p U_\tau}{\vartheta}; \quad \frac{U_p}{U_\tau} = \frac{1}{k}\ln\left(E y_p^+\right); \quad k_p = \frac{U_\tau^2}{\sqrt{C_\mu}}; \quad \varepsilon_p = \frac{U_\tau^3}{k y_p} \quad (9)$$

where, von-Karman constant (k) = 0.41, and linear coefficient (E) = 9.0. Similarly, $u_{1,}$ $k_{1,}$ and ε_1 denoted the resultant parallel wall velocity, kinetic energy, and dissipation rate at the point $y_{1,}$ respectively. Table 1 displays the boundary conditions for the present problem.

3. Methodology

The two-dimensional, steady-state incompressible turbulent flow problem has been attempted to study with different speed ratios, aspect ratios, and Reynolds numbers in an enclosed domain. To study the numerical simulation by using the developed C++ Code. A fine rectangular mesh with a non-uniform grid size discretizes the entire domain while considering the wall effect. Using a finite-volume approach [33], the governing equations are solved by a staggered grid arrangement. A SIMPLE algorithm solves the pressure-velocity coupling equations. The diffusion and convection terms are discretized using Hybrid and Quadratic Upstream Interpolation for Convective Kinematics (QUICK) Schemes[34]. Momentum equations and pressure correction equations are resolved using the tridimensional matrix algorithm (TDMA) and Gauss Siedel, respectively. The iteration is continued till the convergence up to 10^{-8}. The selected parameters are optimized using the Taguchi and ANOVA methods.

4. Results and Discussion

4.1. Grid Independent Study

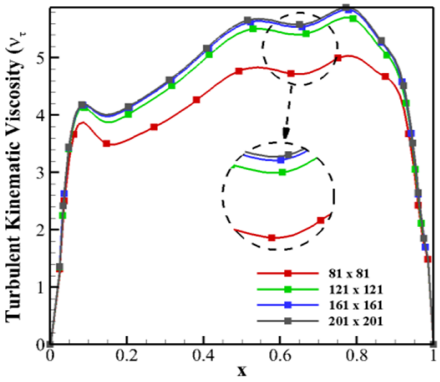

Fig. 2: Grid Independent Study

A grid independence study was conducted to calculate the value of average K, average ε, and average ν_t. The non-uniform mesh is created for this study. To improve the precision of the numerical codes and speed up the execution of the codes, the grid-independent study used five distinct grid sizes: 81×81, 121×121, 161×161, and 201×201, as depicted in Fig. 2 with K=1.0. The number of grids along the x and y-axes are equal to ensure constant grid sizes. By comparing the turbulent viscosity, it has been explicitly proved that the grid size of 161×161 can be selected. Therefore, a 161×161 grid size has been used for the entire computational simulation of the present investigation.

4.2. Code Validation Study

The FVM code validates the existing numerical research by simulating the flow induced by a single lid. Fig. 3 compares centreline velocity profiles with those obtained by a uniform top wall moving solely with a velocity of U_T = 1.0, as reported by Samantaray et al. [35] and Naghian et al.[36]. The excellent agreement between the current study and previous research confirms the validity of the simulation.

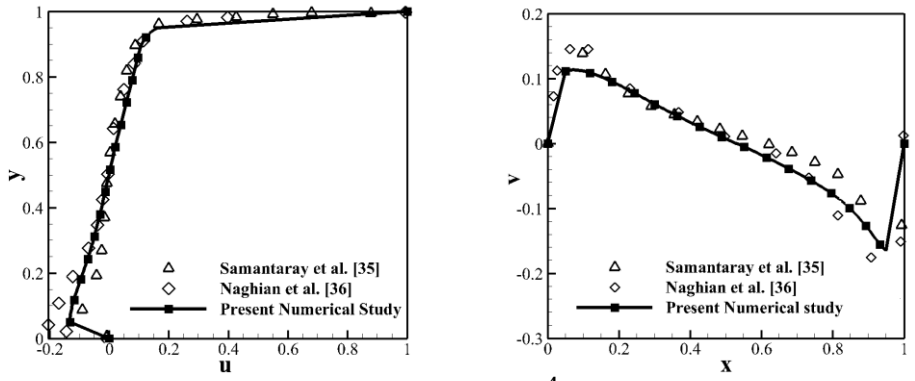

Fig. 3: Comparison of Centreline velocities at Re=1×10^4 and K=1.0 with Samantaray et al. [35] and Naghian et al. [36]

4.3. Effect of S and Re on streamline contours at K =1.0.

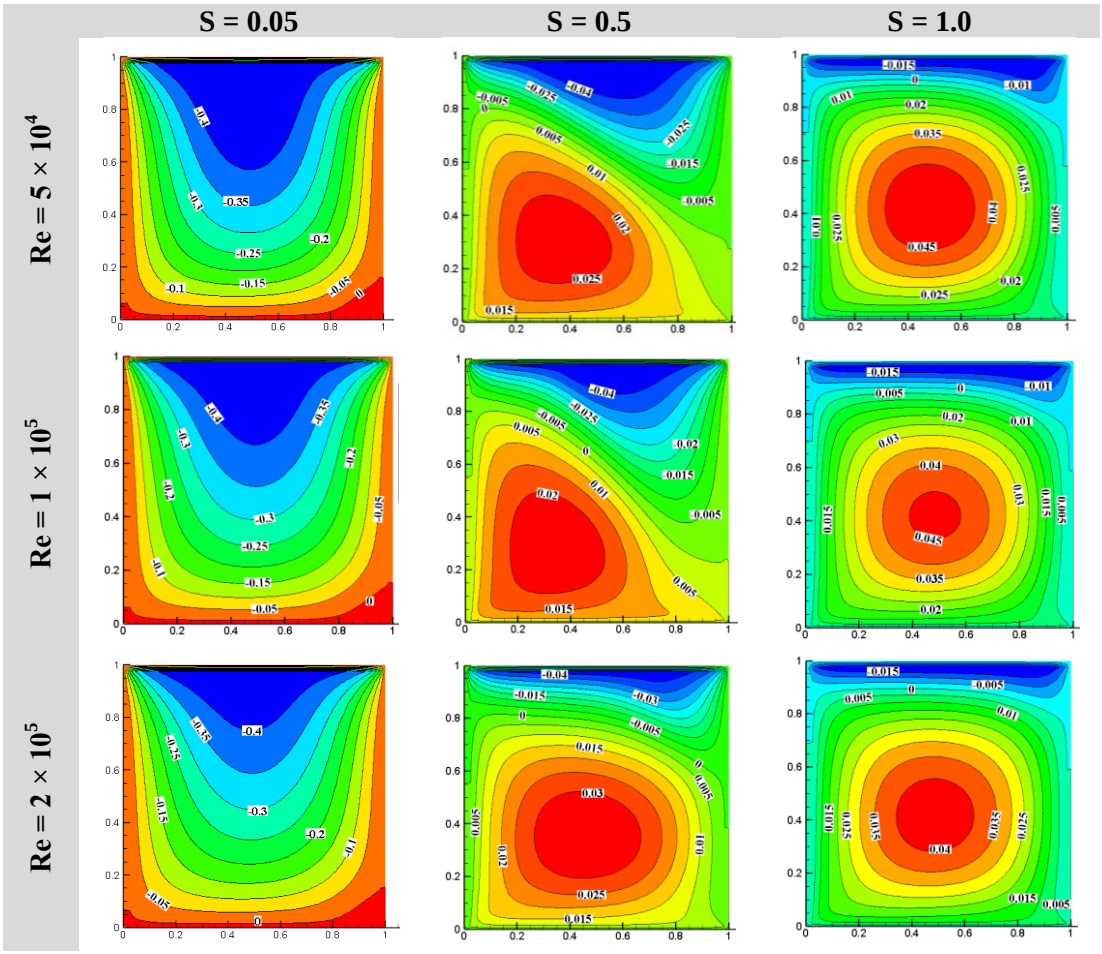

Fig. 4: Effect of Speed ratio and Reynolds number on streamline contours at K=1.0.

Fig. 4 shows the effect of speed ratio and Re on streamline contours for K=1.0. When the speed ratio is 0.05, the top wall velocity is 20 times greater than the bottom wall. In the present study, the horizontal (top and bottom) walls move negatively. Due to this, the streamline contours are rotated in an anticlockwise direction. Hence, the magnitude of the streamline shows a negative value. For this speed ratio, there is no formation of a secondary vortex due to the impact of the top wall velocity being too high. While increasing the speed ratio, the velocity of the top wall decreases, and its effect also decreases. A rapid formation of the secondary vortex occurs, and the primary vortex size decreases with an increase in speed ratio. While the size of the secondary vortex is expanding and

migrating towards the cavity's left side, the primary vortex is getting smaller and shifting upwards. The primary vortex eye moves toward the top side of the cavity while increasing the Reynolds number from 5×10^4 to 2×10^5 for a low-speed ratio. Because the fluid movement is increased due to Re. Therefore, the eye of the secondary vortex is developed and moved toward the center of the cavity by increasing S and Re. For S = 1.0, increasing the Reynolds number causes the secondary vortex to occupy the maximum space of the cavity and pull the primary vortex toward the direction of wall movement.

4.4. Aspect ratio effect on turbulent quantities at Re = 5×10^4 and S=0.05

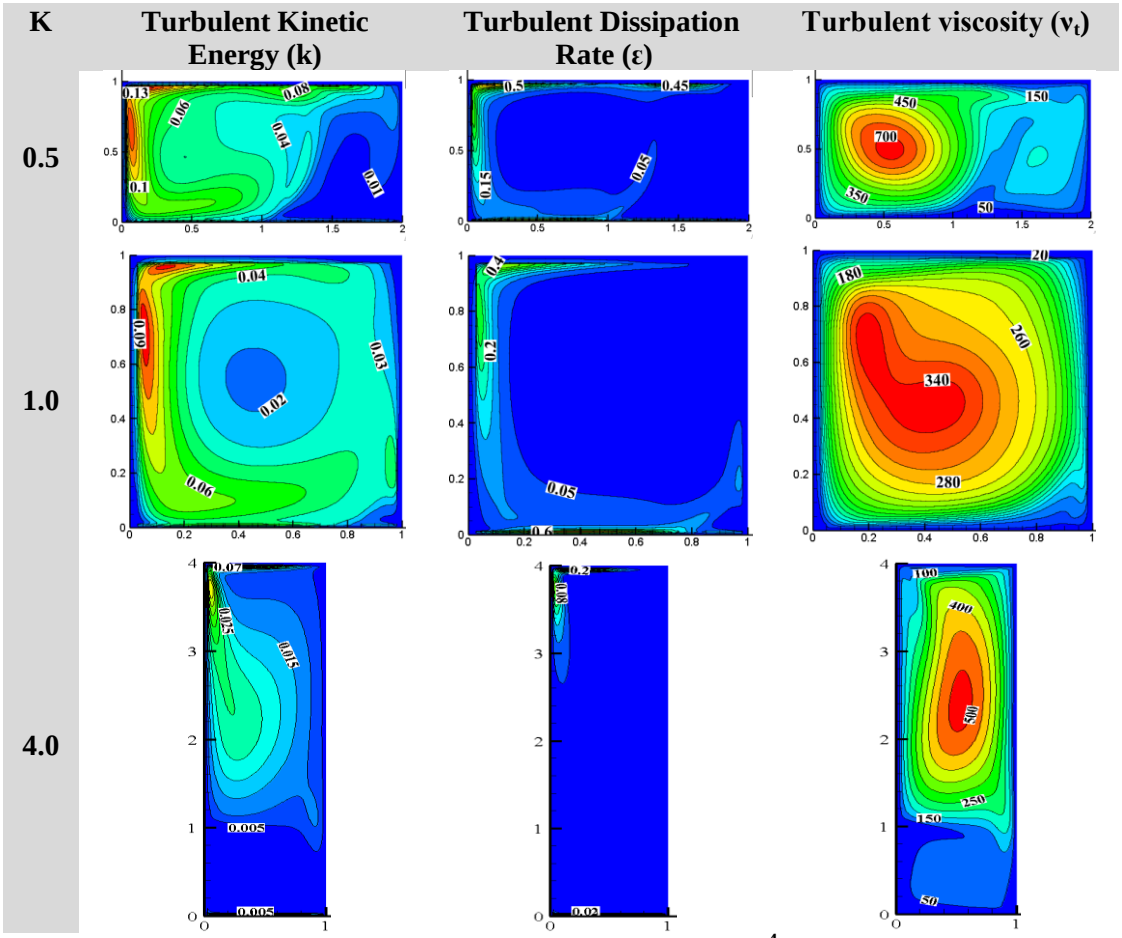

Fig. 5: Effect of aspect ratio on turbulent quantities at Re = 5×10^4 and S=0.05.

Fig. 5 shows the aspect ratio effect on turbulent quantities for Re = 5×10^4 and S=0.05. For K=0.5, the intensity of TKE is higher on the cavity top left because the top wall velocity is higher for the selected speed ratio. Hence, it occupies almost the entire cavity. The dissipation rate occurs only on the top left, dissipating along with the fluid movement. The value of turbulent viscosity depends on both k and ε, and a higher turbulent viscosity is obtained when the ratio of TKE and ε increases. It spreads the entire cavity, and the maximum intensity is near its top left. For all aspect ratios, the maximum TKE intensity is found in the upper left corner, while the lowest is found in the lower right due to the wall movement. As the aspect ratio increases, the concentration of TKE decreases. The maximum TKE is located at K=0.5, and the intensity of TKE decreases and shifts towards the left. However, the intensity diminishes and disperses throughout the cavity when the aspect ratio reaches 4.0. Because the depth of the cavity increases and spreads all over the cavity. For this reason, its

maximum value is decreased from 0.13 to 0.07. The same scenario is followed for the dissipation rate and turbulent viscosity. Near the bottom wall, the concentration of TKE and dissipation rate are less. The turbulent viscosity intensity increases as the K increases. Turbulent quantities follow the same pattern for the same speed ratio and different Reynolds numbers. The pattern has less significance with the increase in the Re effect on the flow, but its intensity is increased for all turbulent quantities. For all aspect ratios, the maximum value TKE and dissipation rate occur near the top wall, where the maximum velocity is also observed. This trend remains consistent while increasing the Re from 5×10^4 to 2×10^5 at S=0.05. TKE is observed to be low, closer to the bottom wall. Higher TKE is shown more prominently on the cavity left side due to the wall movement. Increasing Re to 2×10^5 increases the distribution of TKE, occupying the entire cavity. For Re = 5×10^4, the distribution of the dissipation rate is only on the top left side. While increasing the Re reduces its intensity, the distribution area is more extensive compared to the low range of Re. Increasing the Re, a turbulent dissipation rate forms at the cavity's bottom. In contrast to TKE and dissipation rate, turbulent viscosity increases by increasing the Re, indicating that the flow became more turbulent.

4.5. The effect of Re, S, and K on Turbulent kinetic energy, dissipation, and viscosity.

Fig. 6 shows the effect of Re, S, and K on turbulent quantities. It is more evident from Fig. 6(a) that the turbulent kinetic energy at the horizontal mid-plane is found to be decreased with Re irrespective of S and K. Also, for the range of selected parameters, the kinetic energy is higher near the left wall than the right wall. The magnitude of the TKE is higher for the low-speed ratio, and the oscillation is noticeable because of the low aspect ratio. Similar trends of TKE are observed at a high aspect ratio. However, the change is insignificant and decreases by about 96.52% between S = 0.05 and S = 1.0 at Re =5×10^4, K=0.5. For selected S, the TKE reduces by increasing the aspect ratio from K = 0.5 to 2.0. Overall, it is found that the TKE decreases with the speed ratio for all Re and K. Fig. 6(b) shows the effect of Re, K, and S on turbulent dissipation. Like TKE, the dissipation is also higher near the left wall than the right wall at the horizontal mid-plane. For the selected range of K and S, the dissipation rate of turbulent flow decreases with an increase in Re. Also, for K = 0.5 or 2.0, at any Re, the magnitude of the dissipation is reduced with speed ratio.

Further, the dissipation is decreased with an increase in K for the fixed speed ratio. For Re = 5×10^4 and S = 0.05, the dissipation rate reduces by 85.12% with K=0.5 and 2.0. At S=1.0 and Re=2×10^5, the dissipation rate near the left wall decreases by around 79.54% for K=0.5 and 2.0.

Fig. 6(c) represents the distribution of turbulent viscosity for various Re, S, and K. For K=0.5 and S=0.05, turbulent viscosity follows similar patterns with an increase in intensity by increasing the Re. With an increase in the speed ratio, the intensity of turbulent viscosity is significantly reduced for a selected range of Reynolds numbers because the top wall velocity is reduced according to the speed ratio. When the aspect ratio is 0.5 to 2.0, the maximum intensity of turbulent viscosity decreases for the selected range of Re. The intensity is more concentrated in the middle of the cavity for the low-speed ratio, indicating the existence of a recirculation region inside the cavity. When K=2.0 and Re=5×10^4, the effect of viscosity is more prominent for a low-speed ratio, and it is reduced by increasing the speed ratio. Therefore, it is evident that the speed ratio and Reynolds number affect the distribution of turbulent viscosity. For Re=5×10^4 and K=0.5, the turbulent viscosity is reduced by 88.57% with S=0.05 and 1.0. The Re increases the peak value of turbulent viscosity by 500 to 1750

for Re=5×10^4 and Re=2×10^5 at K=2.0 and S=0.05. At K=2.0 and Re=2×10^5, the turbulent viscosity is reduced by 72.62% for S=0.05 and 1.0.

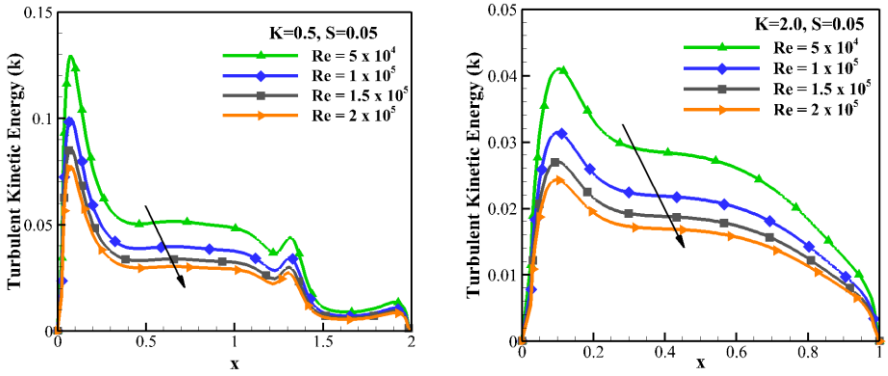

(a) Turbulent Kinetic Energy

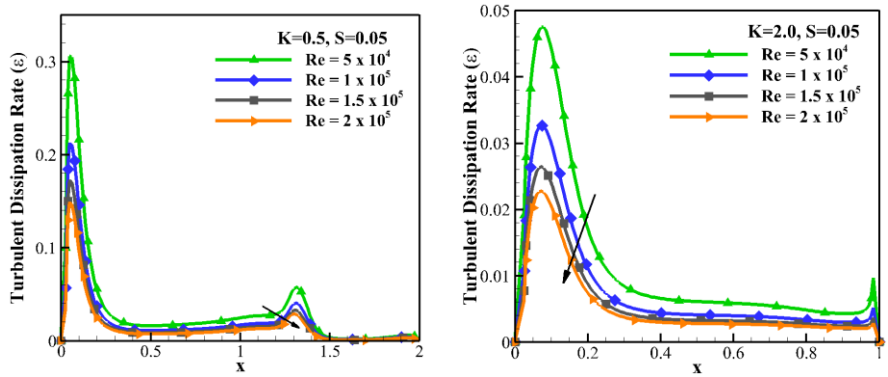

(b) Turbulent dissipation rate

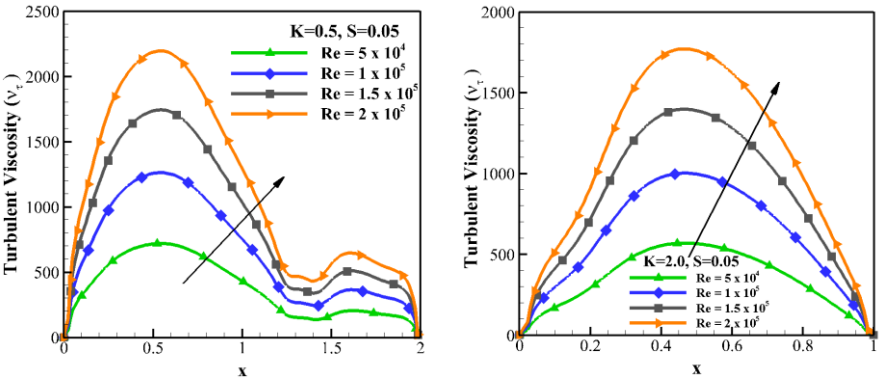

(c) Turbulent viscosity

Fig. 6: The effect of Re, S, and K on turbulent quantities.

4.6. Average turbulent quantities effect for different Re, S, and K

Fig.7 illustrates the influence of average turbulent quantities at various speed ratios and Reynolds numbers, where K is set to 1.0. To identify the quantitative results of turbulent quantities, the horizontal mid-plane is drawn in the cavity from left to right wall, and the turbulent quantities are calculated by a statistical approach using an average of these quantities k_{avg}, ε_{avg}, and $\nu_{t,avg}$. As seen in Fig. 7(a), the average TKE and dissipation rate values decrease as Re increases. Additionally, the turbulent viscosity tends to increase with rising Re. Figs. 7(b) to 7(d) show that the TKE and dissipation rate intensities for the chosen Re range reduce as the speed ratios increase. Conversely, the intensity of turbulent viscosity decreases as the speed ratio increases.

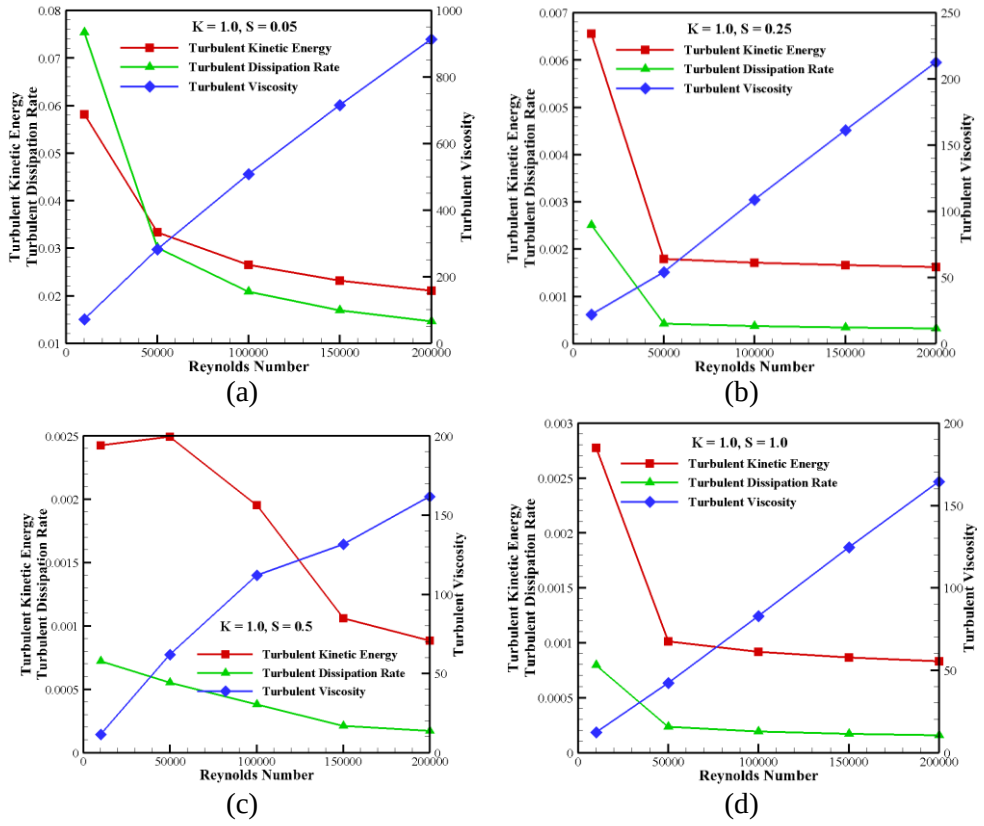

Fig. 7: Effect of Re and Speed ratio on Average turbulent parameters at K=1.0

The analysis shows that the chosen parameters impact turbulent flow characteristics, but it does not provide the significance of each parameter. Therefore, a Taguchi-based optimization study is conducted to examine the performance of dependent parameters. Additionally, ANOVA is employed in the current study to identify the significant variable regulating the maximum turbulent flow characteristics, which are discussed in the following sections.

5. Optimization

5.1. Taguchi Technique

Most analyses require selecting and combining the critical parameters, considering their impact on the output variable. To make this selection, signal-to-noise analysis (S/N) and the findings of an ANOVA table are presented. In this study, Speed ratio (S), Aspect ratio (K), and Reynolds number (Re) have been chosen as independent variables. Based on the governing equations, turbulent viscosity (ν_t) is the function of TKE and dissipation rate. So, the turbulent viscosity has been selected as the dependent variable. To get the quantitative result, the authors took the average value of turbulent viscosity represented by $\nu_{t,avg}$. Various independent factors with four levels were used for the analysis, such as Speed Ratio (0.05, 0.25, 0.5, and 1.0), Reynolds Number (5×10^4, 1×10^5, 1.5×10^5, and 2×10^5), and Aspect Ratio (0.5, 1.0, 2.0, and 4.0). Minitab software is used to identify the selection of an orthogonal array, and an L16 orthogonal array has been decided for the present study. Tab. 3 displays the outcomes of the independent variables combined with their corresponding results. As indicated in Tab. 1, the $\nu_{t,avg}$ for each trial is reported along with S/N ratios. Since the specified array is L_{16}, 16 tests are conducted for the present analysis. The $\nu_{t,avg}$ has been optimized using the larger is the better criterion. The importance of each parameter is determined using ANOVA. Tab. 1 depicts

the $\nu_{t,avg,}$ and S/N ratio for the selected output parameter over all 16 trials using the larger is better for $\nu_{t,avg}$ criterion.

Table 1: Taguchi Orthogonal Array L_{16} and their results

Trial No.	Parameters			Results	
	S	K	Re ($\times 10^5$)	$\nu_{t,avg}$	S/N Ratio
1	0.05	0.5	0.5	284.852	49.092
2	0.05	1.0	1	404.524	52.138
3	0.05	2.0	1.5	654.369	56.316
4	0.05	4.0	2	654.896	56.323
5	0.25	0.5	1	216.720	46.718
6	0.25	1.0	0.5	46.301	33.312
7	0.25	2.0	2	200.572	46.045
8	0.25	4.0	1.5	185.008	45.343
9	0.5	0.5	1.5	209.054	46.405
10	0.5	1.0	2	122.745	41.780
11	0.5	2.0	0.5	59.881	35.545
12	0.5	4.0	1	109.581	40.794
13	1.0	0.5	2	175.149	44.868
14	1.0	1.0	1.5	98.428	39.862
15	1.0	2.0	1	116.902	41.356
16	1.0	4.0	0.5	53.3421	34.541

Tab. 2 shows the results of several parameter combinations, with the optimal ones indicated in bold. The combination of the first level of Speed ratio level (S = 0.05), the first level of aspect ratio (K = 0.5), and the fourth level of Reynolds number (Re = 2×10^5) yields the best cavity performance. S/N ratio responses are calculated for $\nu_{t,avg}$ output parameter, and the results are presented in Tab. 2. The rank displays the relative importance of each factor to the final result. Using the S/N ratio response, the maximum turbulent flow behavior is reached by choosing each parameter's maximum value. For $\nu_{t,avg,}$ the optimal level of the components in the current analysis is S = 0.05, K = 0.5, and Re = 2×10^5. Fig. 8 depicts graphically how each element affects the S/N ratio.

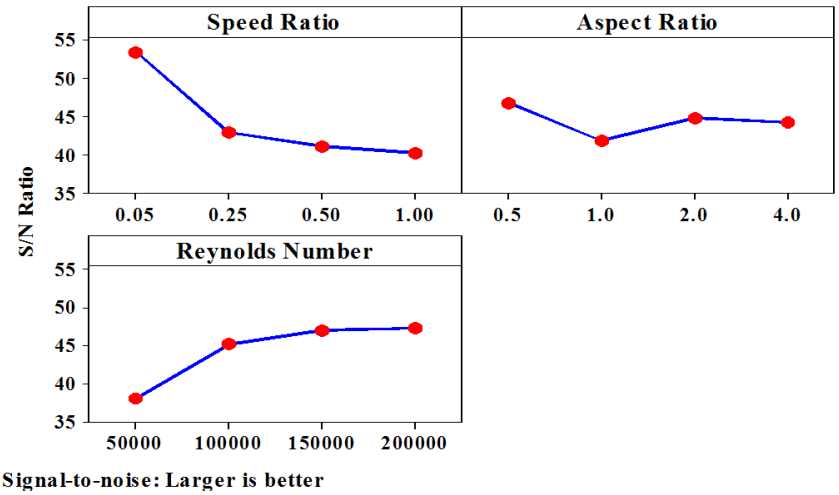

Fig. 8: Independent variables effect on $\nu_{t,avg}$

Table 2: S/N ratio response for $\nu_{t,avg}$

Level	S	K	Re
1	**53.47**	**46.77**	38.12
2	42.85	41.77	45.25
3	41.13	44.82	46.98
4	40.16	44.25	**47.25**
Delta	13.31	5.00	9.13
Rank	1	3	2

5.2. ANOVA technique.

Table 3: ANOVA values for $\nu_{t,avg}$

Source	Degree of Freedom (DOF)	Sum of Square (SS)	Contribution %	Variance	F-Value	P-Value
S	3	453.192	62.29	151.064	243.88	0.001
K	3	50.864	6.99	16.955	27.37	0.015
Re	3	219.766	30.21	73.255	118.26	0.001
Error	6	3.717	0.51	0.619	-	-
Total	15	727.538	100	-	-	-

Applying the ANOVA concept allows one to calculate the relative importance of each component to the dependent variable. Tab. 3 demonstrates how the chosen parameter affected $\nu_{t,avg}$. The investigation shows that S contributes 62.29%, Re contributes 30.21% to increase the flow rate, and K contributes the least to cavity performance. Furthermore, the Taguchi method demonstrates that the ranks of the components are listed in Tab. 2. Fig.11 shows the streamline, turbulent quantities contour for the optimum combination of S = 0.05, K = 0.5, and Re=2×10^5. It is obtained from the Taguchi technique. Contour plots clearly show that the flow rate has increased compared to all other combinations. The average turbulent quantities, such as average TKE (k_{avg}), average dissipation rate (ε_{avg}), and average turbulent viscosity ($\nu_{t,avg}$) for the aforementioned optimal combination are 0.027, 0.025, and 876.204, respectively.

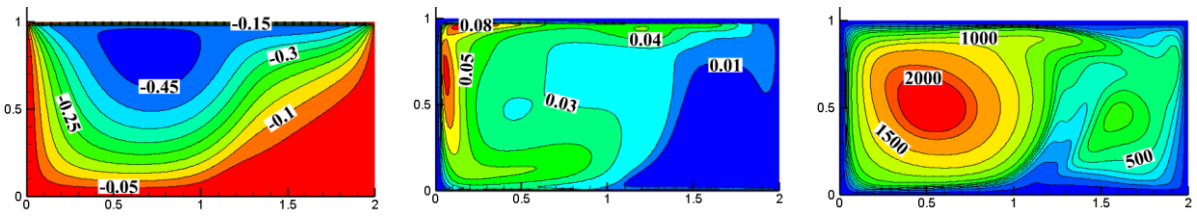

(a) Streamline (b) T.K.E (c) ν_t

Fig. 9: Optimized combination condition contours at S = 0.05, K = 0.5, and Re=2×10^5

5.3. Regression analysis.

The data from Tab. 1 are used in regression analysis to find the model that can accurately predict $\nu_{t,avg}$.

$$\nu_{t,avg} = 190 - 327\,S + 15.8\,K + 0.00121\,Re \quad (10)$$

Nonlinear regression techniques are used to determine the variable coefficients. From the regression analysis, $\nu_{t,avg}$ models are calculated and shown in Eq. (10). The above model only applies to the specifically chosen ranges of variables. The $\nu_{t,avg}$ has a positive relationship with K and Re but a negative one with S.

6. Conclusions

The present study discussed 2D steady-state incompressible turbulent flow characteristics and optimized fluid flow parameters in numerical analyses of the impact of speed ratio, aspect ratio, and Reynolds number. The contours of streamline, turbulence kinetic energy, turbulent viscosity, and dissipation rate are analyzed. From that, the speed ratio controls the influence of lid motion and the secondary corner eddies' strength. A secondary vortex has not formed in the low-speed ratio (S=0.05). The secondary vortex is formed by increasing the speed ratio from 0.25 to 1.0. It reduces the size of the primary vortex. For Re = 5×10^4 and K=1.0, the TKE, dissipation rate, and turbulent viscosity are found to be decreased by 96.35%, 98.79%, and 84.12%, respectively, by varying S from 0.05 to 1.0. Using Taguchi analysis, it is determined that S = 0.05, K = 0.5, and Re=2×10^5 yield the best cavity performance. According to the ANOVA results, the S and Re contribute approximately 62.29% and 30.21%, which are the most influential parameters in deciding the turbulent flow characteristics in the cavity. From the regression equation, $\nu_{t,avg}$ has a positive relationship with both K and Re but a negative relationship with S. The study may be extended to three-dimensional flows, unsteady states, and non-Newtonian fluid used as a working fluid.

Nomenclature

E_1	Linear coefficient	RANS	Reynolds-Averaged Navier-Stokes
G	Production term	LES	Large Eddy Simulation
H	Reference length [m]	DNS	Direct-Numerical Simulation
K	Turbulent kinetic energy	CFD	Computational Fluid Dynamics
K	Aspect ratio	***Greek Symbols***	
P	Pressure [Nm^{-2}]	ε	Dissipation rate
$\overline{p}$	Mean pressure components	ρ	Density [kgm^{-3}]
P	Non- dimensional pressure components	μ	Dynamic viscosity [$Nm^{-2}s^{-1}$)
Re	Reynolds number	ϑ	Kinematic viscosity [m^2s]
S	Speed ratio	***Subscripts***	
u_τ	Frictional velocity [ms^{-1}]	*B*	Bottom
u,v	Velocity components [ms^{-1}]	*i,j*	vector direction
U, V	Non- dimensional velocity components	*n*	non-dimensional
$\bar{u}, \bar{v}$	Mean velocity components	*t*	Turbulent
u', v'	Fluctuating velocity components	*T*	Top
$\overline{u_i' u_j'}$	Reynolds average stress	*avg*	Average
x,y	Cartesian coordinates[m]	*o*	Reference velocity
X, Y	Non- dimensional coordinates		
y^+	Wall function		

Declaration of competing interests

The authors state that they do not have any known financial conflicts of interest or personal relationships that could have been perceived to affect the findings presented in this paper.

Funding

The authors state that they did not receive any funding.

References

[1] Hussien, A.A., W. Al-Kouz, M. El Hassan, A.A. Janvekar, and A.J. Chamkha, A review of flow and heat transfer in cavities and their applications, *European Physical Journal Plus*, *136* (2021), 4.

[2] Alleborn, N., H. Raszillier, and F. Durst, Lid-driven cavity with heat and mass transport, *International Journal of Heat and Mass Transfer*, *42* (1999), 5, pp. 833–853.

[3] Hammami, F., B. Souayeh, N. Ben-Cheikh, and B. Ben-Beya, Computational analysis of fluid flow due to a two-sided lid driven cavity with a circular cylinder, *Computers and Fluids*, *156* (2017), , pp. 317–328.

[4] Shankar, P.N., and M.D. Deshpande, Fluid mechanics in the driven cavity, *Annual Review of Fluid Mechanics*, *32* (2000), , pp. 93–136.

[5] Ghia, U., K.N. Ghia, and C.T. Shin, High-Re solutions for incompressible flow using the Navier-Stokes equations and a multigrid method, *Journal of Computational Physics*, *48* (1982), 3, pp. 387–411.

[6] Erturk, E., T.C. Corke, and C. Gökçöl, Numerical solutions of 2-D steady incompressible driven cavity flow at high Reynolds numbers, *International Journal for Numerical Methods in Fluids*, *48* (2005), 7, pp. 747–774.

[7] Kuhlmann, H.C., M. Wanschura, and H.J. Rath, Flow in two-sided lid-driven cavities: Non-uniqueness, instabilities, and cellular structures, *Journal of Fluid Mechanics*, *336* (1997), , pp. 267–299.

[8] Arun, S., A. Satheesh, and A.J. Chamkha, Numerical Analysis of Double-Diffusive Natural Convection in Shallow and Deep Open-Ended Cavities Using Lattice Boltzmann Method, *Arabian Journal for Science and Engineering*, *45* (2020), 2, pp. 861–876.

[9] Arun, S., and A. Satheesh, Mesoscopic analysis of MHD double diffusive natural convection and entropy generation in an enclosure filled with liquid metal, *Journal of the Taiwan Institute of Chemical Engineers*, *95* (2019), , pp. 155–173.

[10] Mohan, C.G., and A. Satheesh, Computational investigation of double-diffusive mixed convective flow in an enclosed square cavity with soret effect, *Frontiers in Heat and Mass Transfer*, *8* (2017), .

[11] Arun, S., and A. Satheesh, Analysis of flow behaviour in a two sided lid driven cavity using lattice boltzmann technique, *Alexandria Engineering Journal*, *54* (2015), 4, pp. 795–806.

[12] Gaskell, P.H., F. Gürcan, M.D. Savage, and H.M. Thompson, Stokes flow in a double-lid-driven cavity with free surface side walls, *Proceedings of the Institution of Mechanical Engineers, Part C: Journal of Mechanical Engineering Science*, *212* (1998), 5, pp. 387–403.

[13] Albensoeder, S., H.C. Kuhlmann, and H.J. Rath, Multiplicity of steady two-dimensional flows in two-sided lid-driven cavities, *Theoretical and Computational Fluid Dynamics*, *14* (2001), 4, pp. 223–241.

[14] Chen, K.T., C.C. Tsai, W.J. Luo, and C.N. Chen, Multiplicity of steady solutions in a two-sided lid-driven cavity with different aspect ratios, *Theoretical and Computational Fluid Dynamics*, *27* (2013), 6, pp. 767–776.

[15] Hammami, F., N. Ben-Cheikh, B. Ben-Beya, B. Souayeh, N. Ben-Cheikh, and B. Ben-Beya, Combined effects of the velocity and the aspect ratios on the bifurcation phenomena in a two-sided lid- driven cavity flow, *International Journal of Numerical Methods for Heat and Fluid Flow*, *24* (2014), 4, pp. 943–962.

[16] Mendu, S.S., and P.K. Das, Flow of power-law fluids in a cavity driven by the motion of two facing lids - A simulation by lattice Boltzmann method, *Journal of Non-Newtonian Fluid Mechanics*, *175–176* (2012), , pp. 10–24.

[17] Samantaray, D., and M.K. Das, High Reynolds number incompressible turbulent flow inside a lid-driven cavity with multiple aspect ratios, *Physics of Fluids*, *30* (2018), 7.

[18] Patel, D.K., M.K. Das, and S. Roy, LES of incompressible turbulent flow inside a cubical cavity driven by two parallel lids moving in opposite direction, *International Journal of Heat and Mass Transfer*, *67* (2013), , pp. 1039–1053.

[19] Yusof, S.N.A., Y. Asako, N.A.C. Sidik, S.B. Mohamed, and W.M.A.A. Japar, A short review on rans turbulence models, *CFD Letters*, *12* (2020), 11, pp. 83–96.

[20] Abdollahzadeh, M., M. Esmaeilpour, R. Vizinho, A. Younesi, and J.C. Pàscoa, Assessment of RANS turbulence models for numerical study of laminar-turbulent transition in convection heat transfer, *International Journal of Heat and Mass Transfer*, *115* (2017), , pp. 1288–1308.
[21] Milani Shirvan, K., R. Ellahi, S. Mirzakhanlari, and M. Mamourian, Enhancement of heat transfer and heat exchanger effectiveness in a double pipe heat exchanger filled with porous media: Numerical simulation and sensitivity analysis of turbulent fluid flow, *Applied Thermal Engineering*, *109* (2016), , pp. 761–774.
[22] Samantaray, D., and M.K. Das, Nature of turbulence inside a cubical lid-driven cavity: Effect of Reynolds number, *International Journal of Heat and Fluid Flow*, *80* (2019), October, pp. 108498.
[23] Martin, R., M. Soria, I. Rodriguez, and O. Lehmkuhl, On the Flow and Passive Noise Control of an Open Cavity at Re = 5000, *Flow, Turbulence and Combustion*, *108* (2022), 1, pp. 123–148.
[24] Moolya, S., and S. Anbalgan, Optimization of the effect of Prandtl number, inclination angle, magnetic field, and Richardson number on double-diffusive mixed convection flow in a rectangular domain, *International Communications in Heat and Mass Transfer*, *126* (2021), 105358, pp. 1–14.
[25] Alinejad, J., and J.A. Esfahani, Taguchi design of three dimensional simulations for optimization of turbulent mixed convection in a cavity, *Meccanica*, *52* (2017), 4–5, pp. 925–938.
[26] Sobhani, M., and H. Ajam, Taguchi optimization for natural convection heat transfer of Al2O3 nanofluid in a partially heated cavity using LBM, *Journal of Thermal Analysis and Calorimetry*, *138* (2019), 2, pp. 889–904.
[27] Shirvan, K.M., M. Mamourian, and R. Ellahi, Numerical investigation and optimization of mixed convection in ventilated square cavity filled with nanofluid of different inlet and outlet port, *International Journal of Numerical Methods for Heat and Fluid Flow*, *27* (2017), 9, pp. 2053–2069.
[28] Milani Shirvan, K., H.F. Öztop, and K. Al-Salem, Mixed magnetohydrodynamic convection in a Cu-water-nanofluid-filled ventilated square cavity using the Taguchi method: A numerical investigation and optimization, *European Physical Journal Plus*, *132* (2017), 5.
[29] Alinejad, J., and K. Fallah, Taguchi optimization approach for three-dimensional nanofluid natural convection in a transformable enclosure, *Journal of Thermophysics and Heat Transfer*, *31* (2017), 1, pp. 211–217.
[30] Biswas, G., and V. Eswaran, *Turbulent flows: fundamentals, experiments and modeling*, (2002).
[31] Launder, B.E., and D.B. Spalding, *The Numerical Computation of Turbulent Flows*, Pergamon Press, Ltd, (1983).
[32] Nallasamy, M., Turbulence models and their applications to the prediction of internal flows: A review, *Computers and Fluids*, *15* (1987), 2, pp. 151–194.
[33] Patankar, S. V., V.S. Pratap, and D.B. Spalding, Prediction of Turbulent Flow in Curved Pipes, *67* (1975), , pp. 583–595.
[34] Moolya, S., and A. Satheesh, Role of magnetic field and cavity inclination on double diffusive mixed convection in rectangular enclosed domain, *International Communications in Heat and Mass Transfer*, *118* (2020), , pp. 104814.
[35] Samantaray, D., M.K. Das, and D.K. Patel, Turbulence characteristics of high Reynolds number flow inside a three-dimensional cubic lid-driven cavity, *European Journal of Mechanics, B/Fluids*, *84* (2020), , pp. 23–39.
[36] Naghian, M., M. Lashkarbolok, and E. Jabbari, Numerical Simulation of Turbulent Flows Using a Least Squares Based Meshless Method, *International Journal of Civil Engineering*, *15* (2017), 1, pp. 77–87.

Submitted 10.09.2023.

Revised 05.02.2024.

Accepted 07.02.2024.